

ALSS: Apparatus for the loading of sublimable systems

Yuchen Ye(叶育辰), Huixin Hu(胡蕙昕), Jin Zhang(张锦), Francesco Capitani, Mario Santoro, Federico Gorelli, and Philip Dalladay-Simpson

Citation: Chin. Phys. B, 2026, 35 (**7**): 070703. DOI: 10.1088/1674-1056/ae60f2
http://cpb.iphy.ac.cn; http://iopscience.iop.org/cpb

What follows is a list of articles you may be interested in

Gas encapsulation technology for large volume press

Minghao Du(杜明浩) and Duanwei He(贺端威)
Chin. Phys. B, 2024, 33 (**11**): 110701. DOI: 10.1088/1674-1056/ad7af8

Anti-Stokes/Stokes temperature calibration and its application in laser-heating diamond anvil cells

Minmin Zhao(赵旻旻), Binbin Wu(吴彬彬), Jingyi Liu(刘静仪), and Li Lei(雷力)
Chin. Phys. B, 2023, 32 (**9**): 090704. DOI: 10.1088/1674-1056/accd55

In-situ ultrasonic calibrations of pressure and temperature in a hinge-type double-stage cubic large volume press

Qingze Li(李青泽), Xiping Chen(陈喜平), Lei Xie(谢雷), Tiexin Han(韩铁鑫), Jiacheng Sun(孙嘉程), and Leiming Fang(房雷鸣)
Chin. Phys. B, 2022, 31 (**6**): 060702. DOI: 10.1088/1674-1056/ac4902

Investigating the thermal conductivity of materials by analyzing the temperature distribution in diamond anvils cell under high pressure

Caihong Jia(贾彩红), Min Cao(曹敏), Tingting Ji(冀婷婷), Dawei Jiang(蒋大伟), and Chunxiao Gao(高春晓)
Chin. Phys. B, 2022, 31 (**4**): 040701. DOI: 10.1088/1674-1056/ac29aa

Magnetic field analysis in a diamond anvil cell for Meissner effect measurement by using the diamond NV^- center

Lin Zhao(赵琳), Donghui Yue(岳冬辉), Cailong Liu(刘才龙), Min Wang(王敏), Yonghao Han(韩永昊), Chunxiao Gao(高春晓)
Chin. Phys. B, 2019, 28 (**3**): 030702. DOI: 10.1088/1674-1056/28/3/030702

INSTRUMENTATION AND MEASUREMENT

ALSS: Apparatus for the loading of sublimable systems

Yuchen Ye(叶育辰)[1], Huixin Hu(胡蕙昕)[1], Jin Zhang(张锦)[1], Francesco Capitani[2], Mario Santoro[3,4,†], Federico Gorelli[1,5,3,4,‡], and Philip Dalladay-Simpson[1,§]

[1] *Center for High Pressure Science Technology Advanced Research, Shanghai* 201203, *China*
[2] *SOLEIL, L'Orme des Merisiers, Départementale* 128, 91192 *Saint-Aubin, France*
[3] *Instituto Nazionale di Ottica, Consiglio Nazionale delle Ricerche (CNR-INO)*, 50019 *Sesto Fiorentino, Italy*
[4] *European Laboratory for Non Linear Spectroscopy (LENS)*, 50019 *Sesto Fiorentino, Italy*
[5] *Shanghai Advanced Research in Physical Sciences (SHARPS), Shanghai* 201210, *China*

(Received 23 March 2026; revised manuscript received 15 April 2026; accepted manuscript online 17 April 2026)

A system for the loading of sublimable systems at 0 °C into a versatile membrane/screw-actuated symmetric diamond anvil cell (DAC) has been developed. This system, known as the Apparatus for the Loading of Sublimable Systems (ALSS), has the unique incorporation of an internal membrane, which acts against the clamping force of the screws. Through the inflation/deflation of the internal membrane, it is possible to open and close the cell under a pressurized environment without the need to maintain pressure differentials and/or high-pressure mechanical feedthroughs. Here, we present an overview of ALSS and its application in loading sulfur hexafluoride (SF_6) and carbon dioxide (CO_2), including the first infrared absorption measurements of SF_6 up to 50 GPa.

Keywords: diamond anvil cell (DAC), apparatus for the loading of sublimable systems (ALSS)

PACS: 07.35.+k, 91.60.Gf, 92.60.hv, 62.50.–p

DOI: 10.1088/1674-1056/ae60f2 **CSTR:** 32038.14.CPB.ae60f2

1. Introduction

Diamond anvil cells (DACs), since their inception, have played a pivotal role in the development of condensed matter sciences. The DAC's ability to tune density and, consequently, interatomic interactions within a material can significantly modify its physical properties and associated chemistry.[1–8] From a geophysical perspective, the transparency of the anvils and their capacity to probe pressures exceeding those found in Earth's planetary core have long established them as the ideal and perhaps the only window into planetary interiors. The remarkable changes in physical properties are best exemplified by the behavior of hydrogen-rich materials (superhydrides), which have reported superconducting temperatures approaching room temperature, showcasing the power of DACs as a search engine for potentially technologically disruptive materials.[9–11] Given the wide-ranging insights offered by high pressure and the DAC technique, it is imperative to continue developing methodologies for loading materials of physical and geophysical interest to ensure that future investigations are not inhibited.

In high-pressure DAC experiments, the sample to be studied is typically trapped in a diamond vice using a sample chamber, which is a cylindrical hole micromachined into a metallic or ceramic gasket. It is essential that the starting material within this chamber has sufficient density to achieve the desired pressures and/or possesses a sufficiently large sample volume to allow for detailed analysis.[12] Currently, the most common sample loading practices include loading a solid,[4] trapping highly pressurized gas (typically in the kbar range),[7,13–15] or utilizing a liquid,[5,6,16] all of which may be carried out cryogenically and/or under a protective atmosphere. These loading methods can vary significantly in difficulty depending on the material and experimental requirements, and in many cases, experiments may also necessitate a combination of several sample loading techniques.

Systems which undergo sublimation at atmospheric pressure, such as CO_2 and SF_6, present particular challenges for loading into a DAC due to the absence of a liquid phase under cryogenic conditions; they can readily precipitate when used with compressors, rendering standard cryogenic loading impractical and high-pressure gas loading hazardous. Spray loading — cryogenically introducing the solid form of an ambient gas — may also be considered for these systems;[2,3,17] however, it poses several challenges, including: (1) the use of cryogenic liquid (L-N_2), (2) sample contamination, (3) poor sample containment (due to excess sample potentially trapped at the diamond-gasket interface), and (4) difficulty in loading to low pressures. Perhaps the most successful technique for loading systems which undergo sublimation is the combination of low temperatures with a pressure vessel to induce

†Corresponding author. E-mail: santoro@lens.unifi.it
‡Corresponding author. E-mail: federico.gorelli@hpstar.ac.cn
§Corresponding author. E-mail: philip.dalladay-simpson@hpstar.ac.cn

© 2026 Chinese Physical Society and IOP Publishing Ltd. All rights, including for text and data mining, AI training, and similar technologies, are reserved.

the liquid phase;[18] however, this apparatus becomes complicated, requiring mechanical feedthroughs or maintenance of an internal pressure differential on a membrane to clamp the sample between the diamond tips.

In this paper, we introduce the Apparatus for the Loading of Sublimable Systems (ALSS) as an efficient, safe, and contaminant-free procedure for loading a pressure-induced liquid into a diamond anvil cell. We present the loading of CO_2 and SF_6 as prime examples, as these materials hold significant geophysical, quantum chemical, and environmental importance.[8,19–21] The key components of the ALSS methodology include a versatile screw-/membrane-actuated DAC, a pneumatic control system, and a low-temperature bath. A critical aspect of the ALSS design is the incorporation of an internal membrane that counteracts the clamping force of the screws, allowing the diamond anvil cell to be opened and closed within the pressure vessel. This novel approach eliminates the need for mechanical feedthroughs and the maintenance of a pressure differential, which are typically required for the loading of screw-driven and membrane-actuated DACs, respectively. We report the first experimental measurements of the infrared activity of SF_6 at pressures up to 50 GPa, including a novel approach designed to circumvent saturation in absorbance. Although our primary focus is on the loading of sublimable systems, ALSS has also successfully loaded a variety of other systems, including SO_2,[6] NH_3, O_2,[1,5,22] N_2 and Ar, demonstrating its broad applicability.

2. ALSS design

ALSS was designed and fabricated to load systems which do not have a liquidus phase at ambient pressure into DACs under cryogenic and pressurized conditions as safely and cleanly as possible. Its primary design objectives were to withstand 100 bars of internal pressure and to integrate an gas-actuatable membrane for *in-situ* control of the opening/closing of the DAC inside of a pressurised vessel. The design was created using 3D CAD software, which also enabled a finite element analysis (FEA) study. This ensured that we could design ALSS to achieve a safety factor of 8 at its maximum operating pressure while keeping deformations within 10 µm. A general overview of the assembled apparatus is provided in the rendered and cross-sectional schematics of Fig. 1, with an exploded technical drawing and an itemized component list found in Fig. 2 and Table 1.

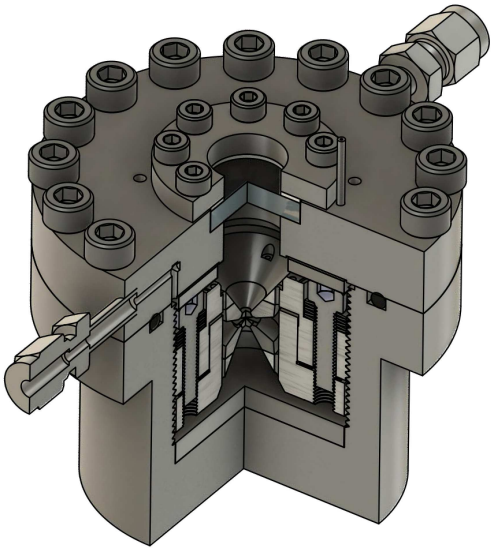


Fig. 1. 3D rendering of ALSS pot with 1/4 cutaway to reveal the DAC as well as the pressure chambers internal structure.

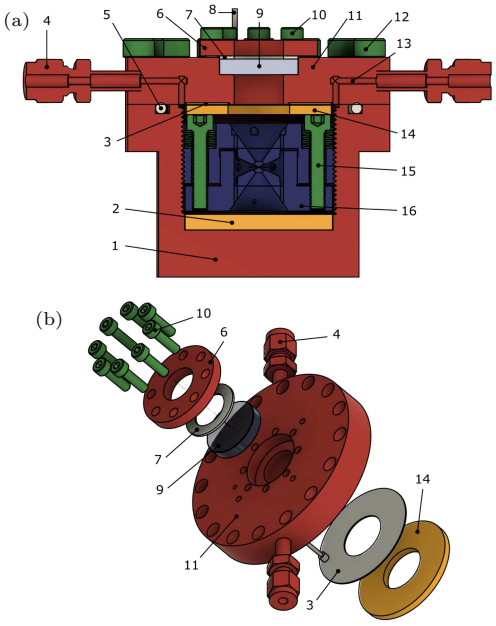


Fig. 2. ALSS design. (a) Cross-sectional view to show interior arrangement of pot. (b) Exploded view of ALSS lid. For part numbers please refer to Table 1.

Table 1. Part numbers and descriptions for the assembly shown in Fig. 2.

No.	Part description	Material
1	ALSS pot	SS 316
2	Spacer	SS 316
3	Laser-welded membrane	SS 316
4	$\frac{1}{4}''$ tube fitting	SS 316
5	O-ring	NBR
6	Window clamp	SS 316
7	Gasket	Teflon
8	$\frac{1}{16}''$ capillary	SS 316
9	$1''$ window	Sapphire
10	M5 bolts	SS 316
11	ALSS lid	SS 316
12	M6 bolts	SS 316
13	Channels for fluid/gas flow	SS 316
14	Pushing plate	SS 316
15	M5 DAC screws	Alloy steel
16	Diamond anvil cell (DAC)	SS 304

The ALSS was CNC machined from a single billet of 316 stainless steel for high strength and corrosion resistance. It consists of two principal components: the ALSS pot and the

ALSS lid, which are sealed and fastened together with sixteen M6 bolts, generating a clamping force sufficient to contain the internal pressure. The pot (colored red in the schematic of Fig. 2(a)) features an internal thread which mates with the external thread of the DAC, allowing for precise vertical adjustment and secure mounting with a positional accuracy of ∼50 µm. The face seal between the pot and lid employs a Nitrile (NBR) O-ring, chosen over materials like Viton due to its superior resistance to permeation and swelling by compressed CO_2, thereby preventing damage from rapid decompression. The lid serves as the primary interface for optical access and gas control, with small internal inlet/outlet channels directly machined into the component. A central sapphire window (Part 9, Fig. 2(b)) permits visual inspection of the sample and monitoring of the liquid condensation. This window is sealed using gaskets comprising a Teflon spacer (Part 6) and a Parafilm sheet seated in a dedicated polished recess in the lid (Part 11). A 1/16″ stainless steel capillary (Part 8, Fig. 2(a)) is laser-welded (leak-free) to the lid to supply high-pressure gas for membrane actuation.

The core innovation of the ALSS is its integrated internal membrane, which enables remote control of the opening/closing of the DAC. Adapted from conventional membrane-driven DACs, this component consists of two laser-welded 200 µm-thick stainless steel foils that form a sealed, inflatable pocket. These membranes have proven to be very robust, routinely withstanding internal pressures of up to 120 bars during our high-pressure DAC experiments. In a typical DAC experiment, such membranes apply force through the DAC body to the diamond anvils, thereby generating pressure on the sample confined between the diamond tips.[23] In our cell design, both the membranes and screws can be used to provide and sustain the loading force. The function of the internal ALSS membrane, however, is inverted: when filled with pressurized helium gas, it generates a load that acts against the clamping force of the DAC's M5 screws, transmitted through the pushing plate and the screw head. This action gently opens the diamond anvil seal, allowing the sample chamber to be flooded by the surrounding pressurized gas within the ALSS pot. Deflating the membrane then re-closes the DAC through the compressed Belleville washers, thereby trapping the sample in the gasket chamber. A detailed operational sequence is provided in Subsection 2.1.

Gas handling for the ALSS is managed by a custom-built, pneumatic control system constructed from Swagelok fittings with tubing diameters ranging from 1/8″ to 1/16″. All pressure gauges and components are rated for at least 200 bar, with digital gauges providing 0.1 bar precision. The system, detailed schematically in Fig. 3, comprises three main modules.

(A) Sample/purge gas inlet Connected to the main ALSS inlet, this module uses a two-way valve to select between two gas cylinders — one containing the sample gas (e.g., SF_6, CO_2) and the other an inert purge gas, helium or argon. A fine needle valve allows for precise control of the inlet pressure and flow rate into the ALSS pot.

(B) Membrane actuation control Dedicated to operating the internal membrane, this line is supplied by a cylinder of inert gas, typically argon, but helium is used if operating in a L-N_2 bath. It features a pressure regulator, inlet/outlet needle valves, a digital pressure gauge, and a ball valve to isolate and maintain a set pressure for stable membrane inflation.

(C) Venting and evacuation Connected to the ALSS outlet, this module includes a digital pressure gauge for monitoring the pot's internal pressure and a needle relief valve for controlled venting, which can be used in tandem with the inlet valve (A) for fine pressure adjustments. A second two-way valve switches the outlet between a vacuum pump (capable of reaching 0.1 mbar) and a vent line exhausted to a fume hood.

The entire system, including all fittings, was rigorously leak-checked with high-pressure helium gas over extended periods prior to operation.

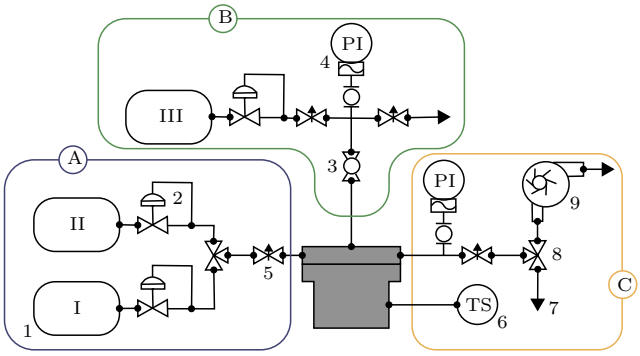


Fig. 3. Pneumatic control diagram for ALSS, with the following numbered parts: (1) gas cylinder, (2) gas regulator, (3) ball valve, (4) digital pressure indicator, (5) needle valve, (6) Pt100 temperature sensor, (7) atmospheric vent, (8) three-way ball valve and (9) rotary vane pump. The system can be divided into three sections: (A) sample/purge gas flow control, (B) membrane inflation control system and (C) venting/evacuation control.

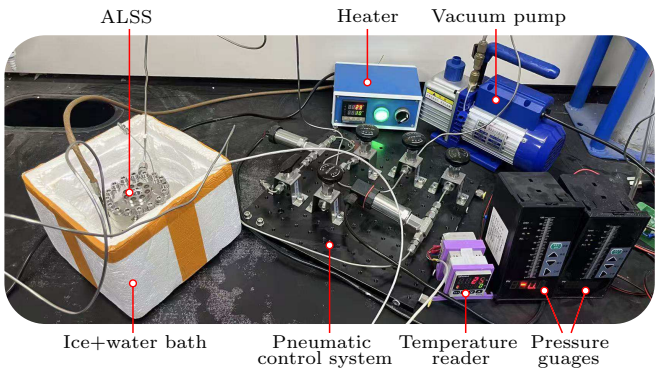


Fig. 4. Photograph of the ALSS experimental configuration inside of a conventional fume hood.

The complete ALSS apparatus is designed to operate within a standard chemical fume hood as seen in Fig. 4. This

containment is essential for the safe handling of toxic, corrosive, or asphyxiant gases, mitigating risks associated with potential leaks during the loading procedure.

2.1. Loading procedure

The following protocol details the procedure for condensing and loading the sublimable systems, CO_2 and SF_6, into the diamond anvil cell using ALSS. All pneumatic controls referenced are shown in Fig. 3 and component numbering corresponds to Fig. 2 and Table 1.

1. Initial DAC preparation Monitor interference fringes from the diamond–gasket interface under a microscope while tightening the DAC screws to achieve initial closure.

2. Chamber assembly Insert the DAC into the loading chamber, ensuring approximately 100 μm clearance between the stainless steel pushing plate (Fig. 2(14)) and the laser-welded membrane (Fig. 2(3)).

3. System evacuation Evacuate ALSS to $\leq$0.5 mbar using the vacuum line (pneumatic control system C in Fig. 3).

4. ALSS inert gas purging Purge ALSS 3–5 times with inert gas (He or Ar) by alternating between evacuation (system C) and gas filling (system A) to remove atmospheric contaminants.

5. Membrane and capillary purging Purge the membrane 3–5 times with He gas via pneumatic control system B (Fig. 3). This step is critical for operations below 273 K to prevent ice blockages in the capillary.

6. Pressurizing ALSS Pressurize the pot to the desired loading pressure: 30 bar for CO_2 or 13 bar for SF_6 using pneumatic control system A (Fig. 3).

7. Temperature equilibration Immerse the assembly in an ice-water bath and allow for thermal equilibration.

8. Cell opening Inflate the membrane to a pressure of 40 bar above the chamber pressure using pneumatic control system B, opening the diamond anvil cell to admit the sample.

9. Sample condensation and monitoring Visually monitor through the sapphire window for gas condensation. Allow the liquid phase to rise above the DAC, ensuring complete immersion of the sample chamber.

10. Cell closure Gradually deflate the membrane to ambient pressure, allowing the force provided by the DAC's clamping screws and Belleville washers to re-close the cell to its initial closed calibration.

11. Pressure release and boiling Remove the assembly from the ice bath and slowly reduce the pot pressure to atmospheric, allowing excess condensed sample to boil off.

12. Final purging and warming Purge the chamber with inert gas (systems A and C) and allow the DAC to warm to room temperature.

13. Post-loading inspection Remove the DAC from the ALSS assembly and inspect the sample with Raman and IR spectroscopy for loading quality and purity (see Figs. 4 and 5 for representative spectra).

This procedure was found to have a 100% success rate for loading systems at 0 °C, including the sublimable systems CO_2 and SF_6. However, for the supplementary loadings noted in Table 2, which required liquid N_2 baths, successful loading is not guaranteed on the first attempt. We believe this is due to substantial differences in frictional forces and/or thermal contraction of the two halves of the DAC at liquid nitrogen temperatures compared to room temperature, meaning the spring force applied by the Belleville washers may be insufficient to close the cell.

3. Experimental results and discussion

Experiments were carried out using symmetric DACs equipped with type IIas diamonds with 200 μm culets. Sample containment was provided by a rhenium foil, with a laser machined cavity with initial dimensions approximately 30 μm in thickness and 60 μm in diameter. Samples were characterized optically using a combination of infrared and Raman spectroscopic diagnostics. Pressure was primarily monitored via ruby fluorescence[24,25] and cross-checked using the Raman-active phonon of the stressed diamond edge.[26]

Raman experiments were carried out using a micro-focused confocal optical system with a 532 nm excitation wavelength. To avoid any unwanted sample heating and/or possible photo-chemistry during the measurements, the incident laser power was kept below 5 mW. The backscattered light was collected and filtered by ultra-narrow holographic notch filters, dispersed by an aberration-corrected spectrometer and imaged by a L-N_2 cooled CCD detector. Measurements were taken using a 1200 gr with exposure times up to 30 seconds to ensure a good signal-to-noise ratio and representative spectra are shown in Figs. 5(a) and 6(a).

In-house IR measurements were carried out using a Bruker Vertex 70v FT-IR interferometer with a Globar MIR source and a KBr beamsplitter. The MIR transmission was focused/captured using a pair of x15 (0.4 NA) Schwarzchild objectives and a L-N_2 cooled mercury cadmium telluride (MCT) detector. All acquisitions were collected in 300 scans and over a frequency range of 400–15000 cm^{-1} with a resolution of 2 cm^{-1}. The in-house infrared absorption spectra are given in Fig. 5(a) for CO_2 and Fig. 6(a) for SF_6.

Synchrotron mid- and far-infrared measurements were conducted on SF_6 at the SMIS beamline using a homemade horizontal microscope in a transmission configuration and are presented as red, blue and black traces in Fig. 7(a). Long-working-distance custom Schwarzschild reflective objectives (0.5 NA) were employed for focusing and collecting the infrared light. The collected light was directed onto either a liquid-He-cooled silicon bolometer (100–900 cm^{-1}) or a

liquid-N_2-cooled MCT detector (650–6000 cm^{-1}) to measure the far- or mid-infrared spectra, respectively. Interferograms were measured by a Fourier-transform Thermo Fisher iS50 spectrometer with a resolution of 2 cm^{-1}. The whole infrared microscope is in a purged environment to minimize atmospheric contributions.

For both in-house and synchrotron infrared measurements, absorption was calculated using an identical cell as a reference, with the two diamond anvils in contact to minimize the interference fringes produced by the Fabry–Perot cavity of an empty gasket hole.

3.1. Carbon dioxide

Carbon dioxide is the archetypal sublimable system, famously coined "dry ice" in 1925, and serves as an excellent benchmark for testing the loading capabilities of the ALSS. The absence of a liquid phase at ambient pressure makes it highly applicable — particularly in the food industry, where it enables cooling without leaving liquid residue. For the same reason, it is also widely used in the medical industry. CO_2 has been extensively studied and exhibits a highly complex phase diagram that parallels that of SiO_2, a major component of the Earth. It adopts different molecular configurations and has the propensity to polymerize under high pressure, forming extended structures with higher oxygen coordination. When compressed at ambient temperature, it provides a classic example of polyamorphism, exhibiting two amorphous states distinguished by their coordination. Annealing at extreme temperatures can yield a cristobalite-like structure, with sharp, well-defined lattice modes. Once formed, this structure is remarkably stable and can persist up to multimegabar pressures and temperatures exceeding 1000 K.[8,27]

CO_2 is not only an archetype for sublimable systems but also for linear molecules. Possessing *Dooh* point group symmetry, it is centrosymmetric with equivalent ends. The carbon atom is double-bonded to two oxygen atoms, and the presence of these double bonds allows for the favourable polymerisation and changes in co-ordination at high pressures. At ambient conditions, the equilibrium bond length is 120 pm, and the bond angle is 180°, resulting in a perfectly linear geometry. A diagram of the equilibrium structure of the CO_2 molecule is shown in the inset of Fig. 5(a). The molecule exhibits four vibrational modes: (1) symmetric stretching (ν_1), (2) doubly degenerate bending (ν_2), and (3) asymmetric stretching (ν_3). Schematics of these modes and their Raman/infrared activities are presented in Fig. 5(b).

CO_2 was loaded at a pressure of 35 bar and 0 °C following the procedure outlined in Subsection 2.1. After allowing the sample to warm to room temperature, representative Raman spectra of the loaded CO_2, in its liquid state at 300 K, are shown in Fig. 5(a). The infrared absorption spectrum (red trace in Fig. 5(a)) reveals two strong features: one corresponding to the degenerate bending mode at approximately 670 cm^{-1}, near the cutoff frequency of our MCT detector (600 cm^{-1}). A strongly absorbing antisymmetric stretching mode is also observed around 2400 cm^{-1}, saturating at an absorbance of approximately 2, which is found to be the detection limit given the sample thickness and geometry. It is important to note that the sharp lines between 1250 cm^{-1} and 2250 cm^{-1} in Fig. 5(a) arise from atmospheric water absorption and are not attributable to the sample.

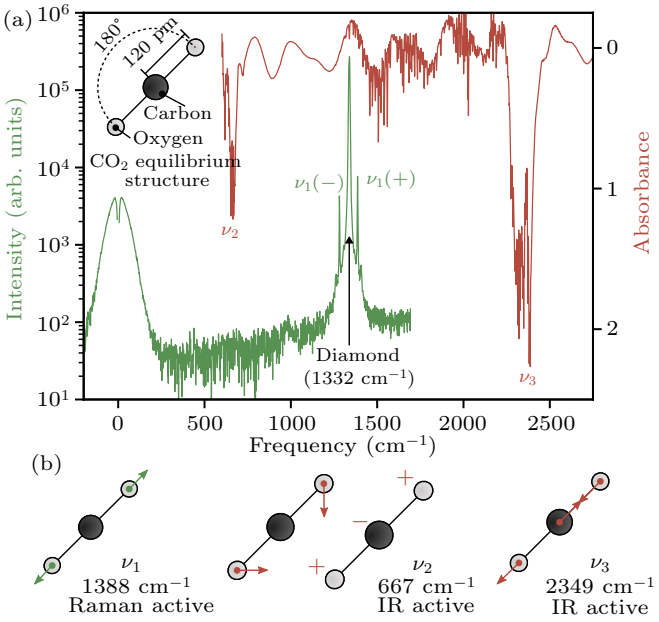


Fig. 5. (a) Raman spectroscopic and infrared measurements from loaded samples of CO_2 at 0.36 GPa and room temperature loaded using ALSS at 35 bars and 0 C. Inset: equilibrium model of the CO_2 molecule. (b) Raman and infrared active normal modes of vibration for the CO_2 molecule and are annotated accordingly in panel (a).

In the Raman spectrum, green trace in Fig. 5(a), we clearly identify the remaining fundamental mode of the CO_2 molecule, the symmetric stretching. It presents as the textbook example of Fermi resonance, a quantum mechanical interaction that splits the vibrational peak into two components, denoted ν^+ and ν^-, which straddle the diamond peak at 1332 cm^{-1}. This feature, known as the Fermi dyad and first identified by Enrico Fermi in 1932, arises from the coincidence in frequencies between the fundamental symmetric stretch (ν_1) and the first overtone of the bending mode ($2\nu_2$). Interestingly, the observed splitting (105 cm^{-1}) has previously been used as a geobarometer to estimate pressures in mineral inclusions.[28,29] Applying this calibration yields an internal pressure of approximately 0.36 GPa in our sample. An additional feature below 250 cm^{-1} is attributed to broadened rotational excitations within the liquid state. After correcting for Bose–Einstein statistics, a Boltzmann-like envelope emerges with a maximum around 20 cm^{-1}, indicating that interactions in the liquid are sufficiently strong to induce collective behavior.

3.2. Sulfur hexaflouride

Coincidentally, SF_6 not only represents an analogous sublimable system to CO_2 but also serves as a pollutant greenhouse gas (GHG) critical to the climate crisis. SF_6 is the most potent GHG known, with a reported effectiveness over a 100-year period estimated to be 23500 times greater than that of CO_2 in capturing infrared radiation. Although only a fraction of SF_6 is produced compared to CO_2, roughly 8100 tonnes per year for SF_6 versus 35 billion tonnes per year for CO_2, once emitted, SF_6 has an extensive atmospheric lifetime of 3200 years.[21] Interestingly, while a significant proportion of CO_2 abundance arises from natural processes, SF_6 is predominantly of anthropogenic origin, with about 80% of synthesized SF_6 used in electric grid infrastructure due to its excellent dielectric and arc-quenching properties. Nonetheless, trace natural sources of SF_6 have been reported in rocks and bodies exposed to volcanic activity. Recent studies indicate that we are on track to achieve a 2.7 °C increase in global temperatures compared to pre-industrial levels by the turn of the century. Investigating the behavior of GHGs under pressure could be vital for modeling new potential chemistries or methods for capturing these gases in stable solid forms, such as in metal–organic frameworks (MOFs)[30] and gas hydrates.[31] Further investigations are crucial for reducing atmospheric GHG levels, which can ultimately lead to severe damage to human and environmental health.

The SF_6 molecule exhibits perfect octahedral geometry belonging to the O_h point group and is therefore analogous to methane (CH_4), characterized by a central sulfur atom bonded to six fluorine atoms positioned at the vertices of a regular octahedron with bond angles of 90°. An equilibrium structure can be found in the inset of Fig. 6(a). Six fundamental vibrational modes are allowed given this molecular structure, of which only two are infrared-active (ν_3 and ν_4) and three are Raman-active (ν_1, ν_2 and ν_5). The ν_6 mode is forbidden in both infrared and Raman spectroscopy. The mutual exclusivity of the infrared and Raman activity in SF_6, as with CO_2, is a classic spectroscopic signature of a molecule with a center of inversion.

SF_6 has been extensively studied at low pressures and over a broad temperature range, as it serves as an excellent model molecule for thermodynamic investigations.[20] Interestingly, at low temperatures, two solid phases are observed:[32] SF_6-I exists from the melting point (224 K) down to 90 K, where it transitions to SF_6-II. These two solid phases have been structurally characterized by neutron diffraction, revealing that phase I adopts a body-centered cubic structure with orientationally disordered molecules — a characteristic "plastic phase." In contrast, phase II consists of orientationally ordered SF_6 molecules arranged in a unit cell containing six molecules. Compared to CO_2, the high-pressure investigation of solid SF_6 remains quite limited, perhaps due to the difficulty associated with loading it into a diamond anvil cell. Pioneering work was first conducted by Stewart, who mapped a discontinuity in volume, a first order phase transition, from his piston displacement experiments from 80–190 K and up to 2 GPa.[33] Later Sasaki *et al.* studied SF_6 using Raman spectroscopy up to 10 GPa at room temperature, and reported liquid–solid and solid–solid transitions.[34] Guided by prior work at lower pressures and temperatures, the solid–solid phase transition was speculatively assigned to SF_6-I and SF_6-II.[33,34] In a more recent study, Rademacher *et al.* unambiguously confirmed this assignment via x-ray diffraction and further identified two additional solid-solid transitions (SF_6-III and SF_6-IV) based on correlated discontinuities in Raman-active modes and Bragg reflections.[35] Notably, in contrast to previous studies, Rademacher *et al.* employed high-pressure gas loading using a dilute SF_6-helium gas mixture.

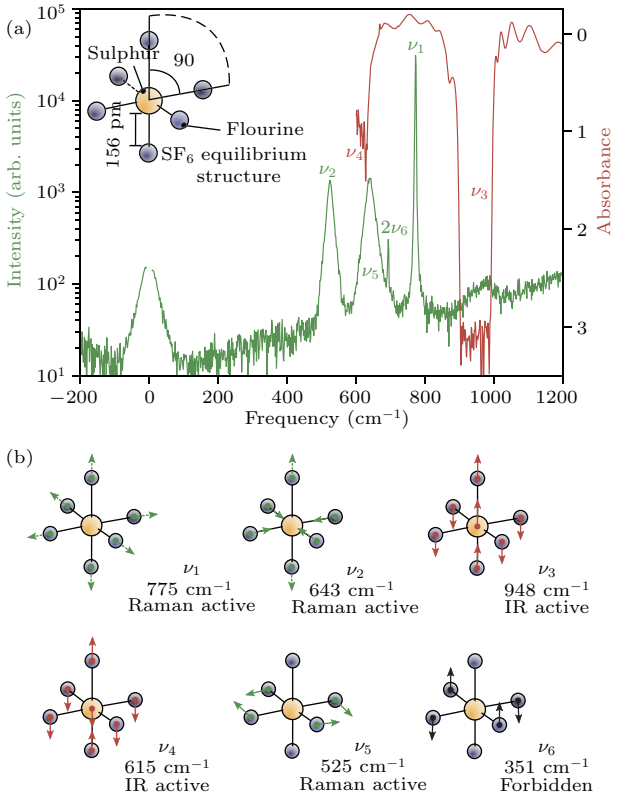


Fig. 6. (a) Raman spectroscopic and infrared measurements of SF_6 at 25 bar and 300 K loaded using ALSS at 15 bar and 273 K. Inset: equilibrium model of the SF_6 molecule. (b) Raman and infrared active normal modes of vibration for the SF_6 molecule and are annotated accordingly in panel (a).

In our experiments, SF_6 was loaded at a pressure of 13 bar and 0 °C following the procedure outlined in Subsection 2.1. After allowing the sample to warm to room temperature, representative Raman spectra of the loaded SF_6 in its liquid state at 300 K are shown in Fig. 6(a). The infrared absorption spectrum (red trace in Fig. 6(a)) reveals two strong features assigned to the vibrations ν_3 and ν_4 at frequencies around

600 cm^{-1} and 950 cm^{-1}, respectively. The latter reaches a saturation of 3 in absorbance, demonstrating the strong infrared cross-section of this mode, which is directly related to its potency as a greenhouse gas. In the Raman spectrum, three distinct vibrations are observed at 525 cm^{-1}, 636 cm^{-1}, and 773 cm^{-1} and are assigned to the fundamental modes of the molecule ν_2, ν_5, and ν_1 respectively. Interestingly, we also observe a sharp mode at 693 cm^{-1}, and due to a coincidence of the frequency, we assign it to the second order of the forbidden ν_6 mode. Interestingly, at low frequency a tail is found to extend to 80 cm^{-1} around the Rayleigh line; due to the symmetry of the SF_6 molecule, the rotational modes for isolated/gas molecules are forbidden, and therefore the appearance of this mode is likely a consequence of interactions and collective behavior among the molecules in the liquid.

Figure 7 presents the first infrared measurements of SF_6 at high pressures up to 50 GPa and room temperature. We show spectra of the solid (blue traces), phase I (red trace), and the ordered phases (phase II/III/IV, black traces). As can be seen, the fundamental vibrational modes ν_3 and ν_4 remain saturated throughout the entire compression, which makes identifying peak frequencies impossible. These saturated bands are plotted as bars in Fig. 7(c). No infrared absorption was observed in the far-infrared regime, which is consistent with reports in the Raman spectra, where no optical phonons were observed.[34] However, additional weak absorptions, OD <0.01 (filled black circles in Fig. 7(c)), observed around 557 cm^{-1}, 689 cm^{-1} and 825 cm^{-1} at 20.7 GPa, were found in the ordered phases. Given their steeper pressure dependence and inherently weak cross-section relative to the fundamental excitations, these could represent combination modes involving crystal phonon absorptions.

To circumvent saturation, we developed a method, shown in Fig. 7(b), which employed the addition of a thin stainless steel ring of 5 μm thickness to be filled with liquid SF_6. The remainder of the gasket chamber was prepared in the usual fashion for high-pressure experiments and packed with KBr, which is highly transparent in the infrared. This approach provided a sufficiently thin sample to avoid saturation while maintaining an adequate gasket thickness to ensure mechanical stability of the DAC up to the highest pressures.

The stainless steel shim was prepared from a large foil of highly uniform 5 μm thickness. The disc was cut out using a pulsed laser trepanning system, the same system used to drill the sample chamber in the Re gasket. This drilling system consists of a rotation stage and two X–Y translation stages, allowing alignment of the laser to the center of rotation as well as offset control for precision machining of circles of various diameters. First, the central hole (corresponding to the diameter of the hole in the Re gasket) was machined, followed by a larger circle matching the culet diameter, which released the ring from the bulk sheet. Wax was used to maintain the foil's position on a glass slide and prevent loss of the small disc during drilling. The sample chamber in the Re gasket was packed with dry KBr and compressed until the chamber appeared homogeneous. The DAC was then opened again, and the excess KBr was removed from the gasket and diamond surfaces. The stainless steel shim was then manually placed onto the diamond tip using a needle, and the DAC was closed again under the microscope, with care taken to ensure that the gasket sealed well without applying enough force to compress the sample chamber.

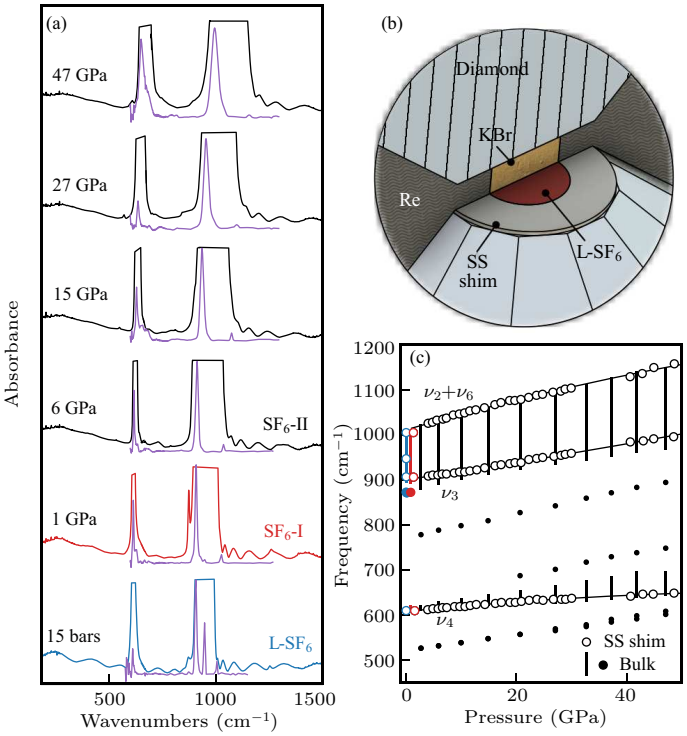


Fig. 7. Infrared spectroscopy of SF_6 up to 50 GPa. (a) Representative IR absorption spectra up to 50 GPa. Blue, red and black traces are used to indicate the liquid, phase I and orientationally ordered phases (II/III/IV), respectively. Purple traces indicate measurements done using a thin stainless steel shim, shown in panel (b), to avoid peak saturation in absorption. (b) Schematic of the experimental set-up to avoid saturation in absorption, a cross-section of the top anvil and Re-gasket is made for clarity. Here the liquid SF_6, red in the figure, fills the cavity in the stainless steel shim ∼5 μm in thickness and sealed at 15 bars and 0 °C. The chamber made in the Re-foil is packed with dry KBr, colored orange in this figure, which does not have strong infrared activity. (c) Absorptions as a function of pressure, bars represent frequency ranges which are saturated and filled black symbols weak absorptions (OD< 0.01), both from bulk SF_6 loadings. Empty symbols represent frequencies extracted using the SS shim technique and red, blue and black are from the liquid, phase I and the orientationally ordered SF_6 phases (II/III/IV), respectively.

The spectrum produced from this technique is shown by the purple traces in Fig. 7(a), and the extracted frequencies are plotted as a function of pressure in Fig. 7(c) as empty circles. Using this method, we extracted the combination band, which is assigned to $\nu_2 + \nu_6$ based on frequency coincidence. Additionally, in the liquid phase, an extra absorption is observed at 946 cm^{-1} and is assigned to a small gaseous component of SF_6 remaining in the KBr sample after loading. Interestingly, de-

spite previous claims of several solid–solid phase transitions at higher pressures, namely phases III and IV, all excitations were found to increase monotonically with pressure, providing no additional evidence for structural transitions.

3.3. Other systems

Beyond loading sublimable systems, this apparatus has proven effective for the loading of high-purity cryogenic liquids into a DAC.[1,5,6,22] A summary of the systems loaded and the corresponding thermodynamic conditions is provided in Table 2.

Table 2. Cryogenic loading conditions for other ambient condition gases.

System	Pressure (bars)	Temperature (K)
SO_2	5	300
NH_3	5	273
O_2	10	120
N_2	10	100
Ar	10	115

4. Conclusion

In summary, we have designed, constructed, and validated the Apparatus for Loading Sublimable Systems (ALSS), a specialized instrument that solves the problem of loading high-purity samples that require pressurized and/or cryogenic conditions to achieve a liquid state for loading in a DAC. The key innovation lies in its internal membrane for *in-situ* cell control, actuating the DAC opening/closing in the pressurised environment. We have demonstrated its efficacy by loading two fundamental systems: CO_2, as a benchmark, and SF_6, for which we report the first infrared spectra under compression to 50 GPa at room temperature. Beyond these proof-of-principle sublimable systems, the ALSS design — particularly its operation within a fume hood and its leak-tested gas handling — provides a critical safety framework for studying hazardous materials. Thus, this instrument adds a versatile and safe new option to the high-pressure researcher's toolkit.

Acknowledgements

The authors acknowledge SOLEIL synchrotron and the SMIS beamline for their support during the experiments conducted under proposal 20240376. P. D-S. acknowledges the support of the National Natural Science Foundation of China (Grant No. W2532012).

References

[1] Dalladay-Simpson P, Monserrat B, Zhang L and Gorelli F 2024 *Matter and Radiation at Extremes* **9** 028401
[2] Dalladay-Simpson P, Binns J, Peña-Alvarez M, Donnelly M E, Greenberg E, Prakapenka V, Chen X J, Gregoryanz E and Howie R T 2019 *Nat. Commun.* **10** 1134
[3] Binns J, Hermann A, Peña-Alvarez M, Donnelly M E, Wang M, Kawaguchi S I, Gregoryanz E, Howie R T and Dalladay-Simpson P 2021 *Sci. Adv.* **7**
[4] Ma Y, Eremets M, Oganov A R, Xie Y, Trojan I, Medvedev S, Lyakhov A O, Valle M and Prakapenka V 2009 *Nature* **458** 182
[5] Gorelli F A, Dalladay-Simpson P, Garbarino G, Mezouar M, Haines J and Santoro M 2025 *Phys. Rev. Lett.* **135** 076101
[6] Zhang H, Dalladay-simpson P, Santoro M, Gorelli F A, Capitani F, Ji C and Zhang L 2025 *Commun. Chem.* **8** 374
[7] Dalladay-Simpson P, Howie R T and Gregoryanz E 2016 *Nature* **529** 63
[8] Santoro M, Gorelli F A, Bini R, Ruocco G, Scandolo S and Crichton W A 2006 *Nature* **441** 857
[9] Ashcroft N W 2004 *Phys. Rev. Lett.* **92** 187002
[10] Drozdov A P, Kong P P, Minkov V S, Besedin S P, Kuzovnikov M A, Mozaffari S, Balicas L, Balakirev F F, Graf D E, Prakapenka V B, Greenberg E, Knyazev D A, Tkacz M and Eremets M I 2019 *Nature* **569** 528
[11] Drozdov A P, Eremets M I, Troyan I A, Ksenofontov V and Shylin S I 2015 *Nature* **525** 73
[12] Dewaele A, Loubeyre P, Occelli F, Marie O and Mezouar M 2018 *Nat. Commun.* **9** 2913
[13] Dalladay-Simpson P, Capitani F and Gorelli F A 2025 *Phys. Rev. B* **112** 014102
[14] Rivers M, Prakapenka V B, Kubo A, Pullins C, Holl C M and Jacobsen S D 2008 *High Pressure Research* **28** 273
[15] Kurnosov A, Kantor I, Boffa-Ballaran T, Lindhardt S, Dubrovinsky L, Kuznetsov A and Zehnder B H 2008 *Rev. Sci. Instrum.* **79** 045110
[16] Edmund E, Dalsaniya M H, Howie R T, Greenberg E, Prakapenka V B, Peña Alvarez M, Hanfland M, Dalladay-Simpson P, Kurzydłowski D and Hermann A 2025 *Phys. Rev. B* **112** 134101
[17] Scelta D, Ceppatelli M, Ballerini R, Hajeb A, Peruzzini M and Bini R 2018 *Rev. Sci. Instrum.* **89**
[18] Baggen M, Manuputy R, Scheltema R and Lagendijk A 1988 *Rev. Sci. Instrum.* **59** 2592
[19] An M, Prinn R G, Western L M, Zhao X, Yao B, Hu J, Ganesan A L, Mühle J, Weiss R F, Krummel P B, O'Doherty S, Young D and Rigby M 2024 *Nat. Commun.* **15** 1
[20] Hurly J J, Defibaugh D R and Moldover M R 2000 *International Journal of Thermophysics* **21** 739
[21] Kovács T, Feng W, Totterdill A, Plane J M, Dhomse S, Gómez-Martín J C, Stiller G P, Haenel F J, Smith C, Forster P M, García R R, Marsh D R and Chipperfield M P 2017 *Atmospheric Chemistry and Physics* **17** 883
[22] Frost M, Kuzovnikov M A, Dalladay-simpson P, Howie R T, Loveday J S, Ranieri U and Gregoryanz E 2025 *Commun. Chem.* **8** 128
[23] Letoullec R, Pinceaux J P and Loubeyre P 1988 *High Pressure Research* **1** 77
[24] Shen G, Wang Y, Dewaele A, Wu C, Fratanduono D E, Eggert J, Klotz S, Dziubek K F, Loubeyre P, Fat'yanov O V, Asimow P D, Mashimo T and Wentzcovitch R M 2020 *High Pressure Research* **40** 299
[25] Datchi F, Dewaele A, Loubeyre P, Letoullec R, Le Godec Y and Canny B 2007 *High Pressure Research* **27** 447
[26] Akahama Y and Kawamura H 2006 *J. Appl. Phys.* **100**
[27] Goncharov A F, Bykova E, Bykov M, Edmund E, Smith J S, Chariton S and Prakapenka V B 2023 *Phys. Rev. Mater.* **7** 053604
[28] Sode O, Keçeli M, Yagi K and Hirata S 2013 *J. Chem. Phys.* **138** 074501
[29] Span R and Wagner W 1996 *Journal of Physical and Chemical Reference Data* **25** 1509
[30] Li J, Chen Y, Ke T, Jin Y, Fan R, Xu G, Yang L, Zhang Z, Bao Z, Ren Q and Yang Q 2025 *Nat. Commun.* **16** 632
[31] Dyadin Y A, Larionov E G, Manakov A Y, Kurnosov A V, Zhurko F V, Aladko E Y, Ancharov A I, Tolochko B P and Sheromov M A 2002 *Journal of Inclusion Phenomena* **42** 213
[32] Cockcroft J K and Fitch A N 1988 *Zeitschrift für Kristallographie - Crystalline Materials* **184** 123
[33] Stewart J W 1962 *J. Chem. Phys.* **36** 400
[34] Sasaki S, Tomida Y and Shimizu H 1992 *J. Phys. Soc. Jpn.* **61** 514
[35] Rademacher N, Friedrich A, Morgenroth W, Bayarjargal L, Milman V and Winkler B 2015 *Journal of Physics and Chemistry of Solids* **80** 11